Improved Tumor Penetration and Single-Cell Targeting of Antibody Drug Conjugates Increases Anticancer Efficacy and Host Survival

Cornelius Cilliers[*], Bruna Menezes[*], Ian Nessler[*], Jennifer Linderman[*#], and Greg M. Thurber[*#]

[*] Department of Chemical Engineering, University of Michigan, Ann Arbor, MI 48109

[#] Department of Biomedical Engineering, University of Michigan, Ann Arbor, MI 48109

Supplementary Data

Supplementary Figures

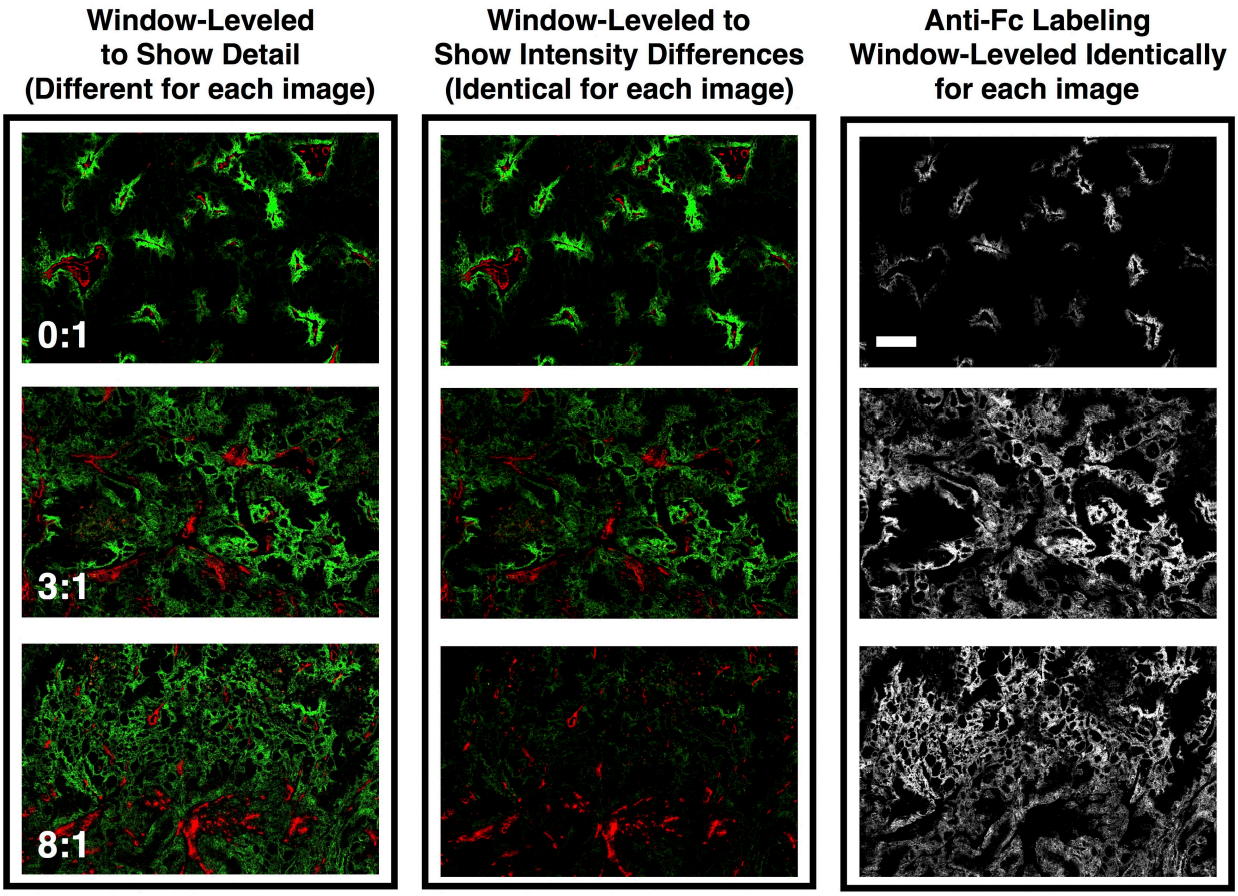

Figure S1 – Improving T-DM1 tumor distribution through co-administration of trastuzumab. Similar to Fig. 1, administration of T-DM1 at 3.6 mg/kg (single agent) results in a heterogeneous, perivascular distribution due to rapid binding relative to transport in the tissue (*top row*). T-DM1 distribution is improved when co-administered with a subsaturating (*middle row*) or saturating (*bottom row*) dose of trastuzumab. The left and middle column shows distribution of AF680 labeled T-DM1 (*green*) at 3.6 mg/kg with unlabeled trastuzumab at 0:1, 3:1, and 8:1 trastuzumab:T-DM1 ratios (0, 10.8, and 28.8 mg/kg, respectively). Microscope settings and window leveling are identical for the top row, middle row, and bottom row images in the middle column to show differences in intensity (less ADC per targeted cell), while the images of the top, middle, and bottom rows of the left column are window leveled to highlight the better tumor penetration of ADC. Immunofluorescence staining with CD31-AF488 (*red*) shows the tumor vasculature. The right column shows immunofluorescence staining with antihuman IgG Fc-AF555 (*gray*). All tumors were resected 24 hours after injection. Scale bar is 200μm.

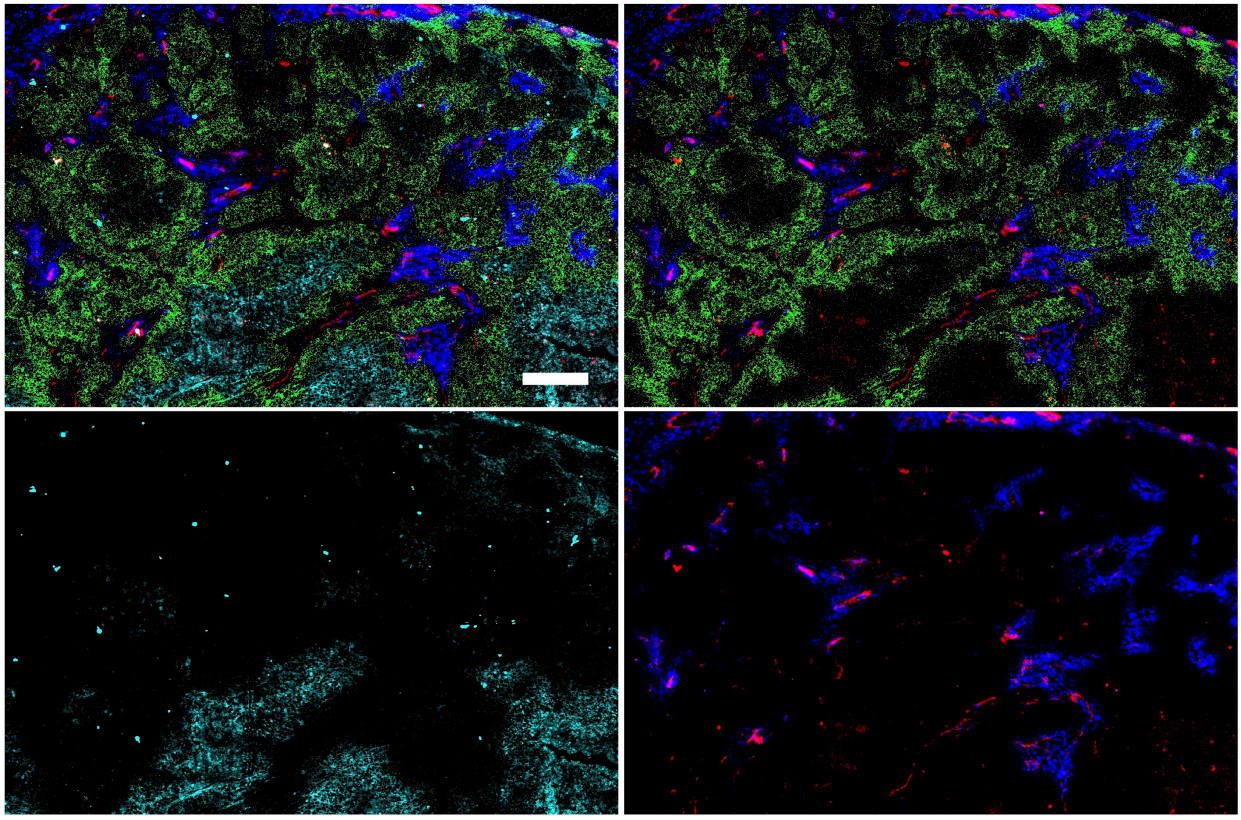

Figure S2 – Immunofluorescence histology of T-DM1-800 (green) dosed at 14.4 mg/kg (same total antibody dose as 3:1 trastuzumab:T-DM1 ratio). Hoechst 33342 (blue) was injected prior to sacrifice to stain functional vasculature as outlined in Materials and Methods. CD31-555 (red) and trastuzumab-AF488 (cyan) were stained *ex vivo*. Trastuzumab only binds free receptors in regions not targeted by T-DM1 at this time point. Similar to increasing the dose of trastuzumab, tumor penetration is improved with higher doses of single agent T-DM1. Although tumor penetration is improved with higher ADC doses, ADC toxicity limits the maximum tolerated dose. Top left, all stains; top right, T-DM1 (green), Hoecsht 33342 (blue), and CD31 (red); bottom left, free HER2 antigen (trastuzumab *ex vivo*, cyan); bottom right, Hoechst and CD31. Scale bar is 200 μm.

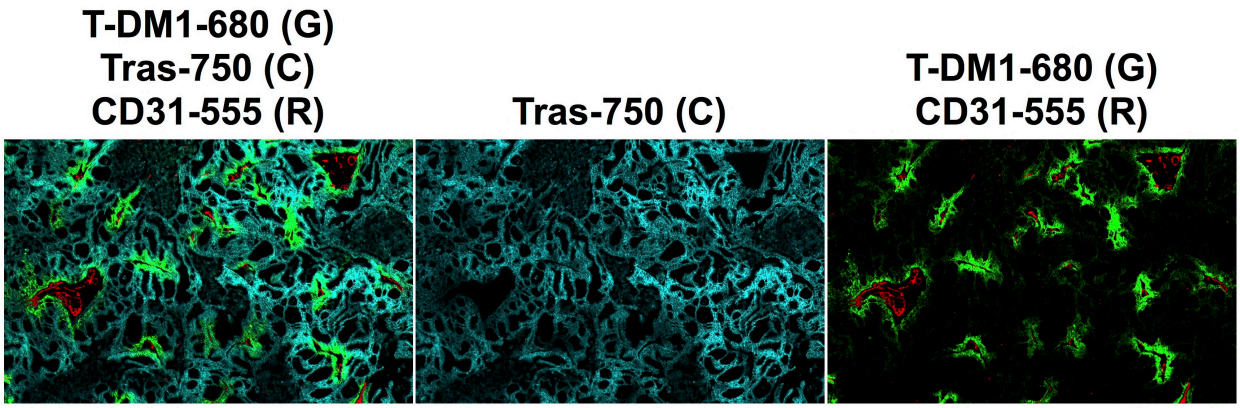

Figure S3 – Immunofluorescence histology of HER2 antigen. Slices were stained with trastuzumab-AF750 to ensure the perivascular distribution of T-DM1-AF680 was not from a lack of available antigen farther from the vessels. The left column shows a merge of T-DM1-680 (green), trastuzumab-750 (cyan), and CD31-555 (red). The middle and right columns show unmerged images of trastuzumab-750 and T-DM1-680 with CD31, respectively. Tras, trastuzumab; G, green; C, cyan; R, red.

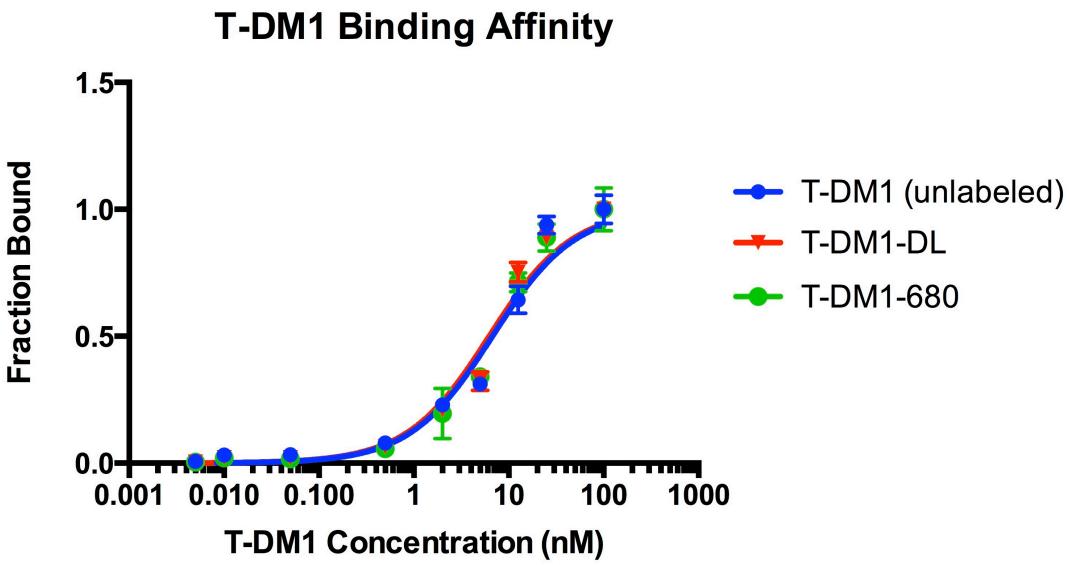

Agent	K_d (nM)
T-DM1 (unlabel)	6.7 ± 1.1
T-DM1-680	6.2 ± 1.0
T-DM1-DL	6.4 ± 0.9

Figure S4 – T-DM1 dye conjugate binding affinity. Conjugation of fluorophores to T-DM1 at a dye-to-protein ratio of 0.3 or less did not affect T-DM1 binding affinity. Binding affinity was performed as previously described(1,2). Briefly, concentrations of unlabeled antibody and antibody−dye conjugates were incubated with 50,000 HCC1954 cells on ice for 3 hours and washed with PBS. After the primary incubation, cells were further incubated with antihuman IgG Fc-AlexaFluor488 at 40 nM for 30 min on ice, then washed with PBS, and subsequently analyzed on an Attune Focusing Cytometer (Applied Biosystems). K_d was calculated using PRISM and is reported as K_d ± standard error. DL, dual-label (both IRDye and DDAO); 680, AlexaFluor680.

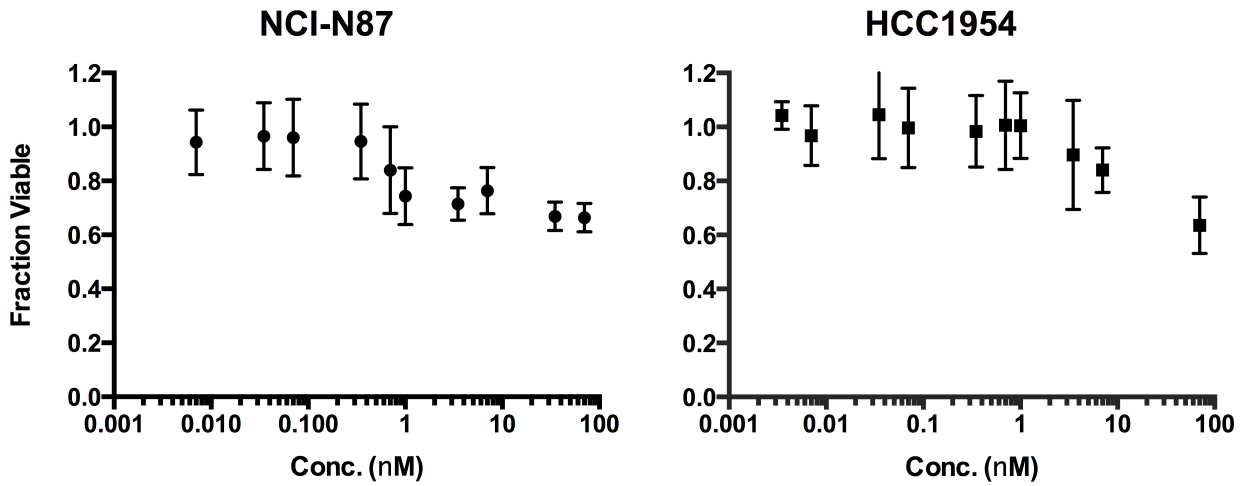

Figure S5 – *In vitro* toxicity of trastuzumab alone. NCI-N87 and HCC1954 cells were incubated with trastuzumab titrations over 6 days. Consistent with literature reports that these cell lines are resistant to trastuzumab, both cell lines showed only limited growth inhibition at the highest concentrations.

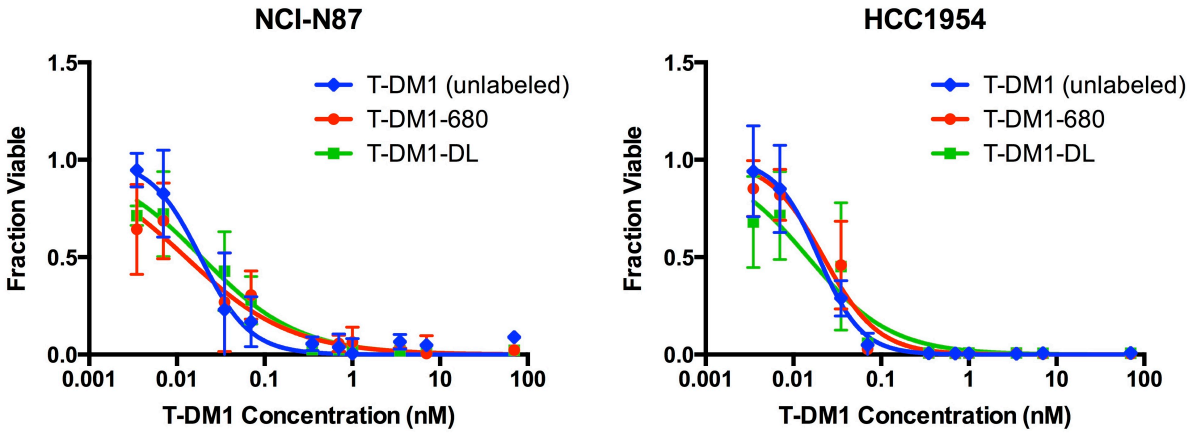

ADC Dye Conjugate	IC50 (pM)	95% Confidence Intervals (pM)
T-DM1 (unlabel)	19	14 to 25
T-DM1-680	13	8 to 21
T-DM1-DL	19	14 to 26

ADC Dye Conjugate	IC50 (pM)	95% Confidence Intervals (pM)
T-DM1 (unlabel)	19	17 to 22
T-DM1-680	22	15 to 32
T-DM1-DL	15	9 to 25

Figure S6 – Dye conjugation to T-DM1 does not affect *in vitro* cytotoxicity. Similar to Figure 2, NCI-N87 (left) and HCC1954 (right) cells were incubated with varying concentrations of T-DM1 or T-DM1 dye conjugates for six days, replacing the media daily. IC50 and 95% confidence interval was estimated using PRISM and is reported below each plot. DL, dual-label (both IRDye and DDAO); 680, AlexaFluor680.

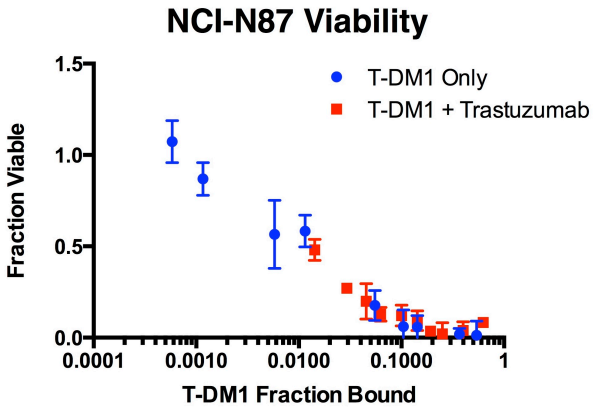

Figure S7 – NCI-N87 cell viability data fit with a competitive binding model. Using the affinity data from Figure S8 and our previous work with trastuzumab(1), we estimated the fraction bound of T-DM1 alone (Fig. 2A) and T-DM1 with trastuzumab (Fig. 2B) using a simple competitive inhibition binding model. Although adding trastuzumab increased the IC50 in Fig. 2C, cell viability was similar when adjusting to the fraction of receptors bound by T-DM1.

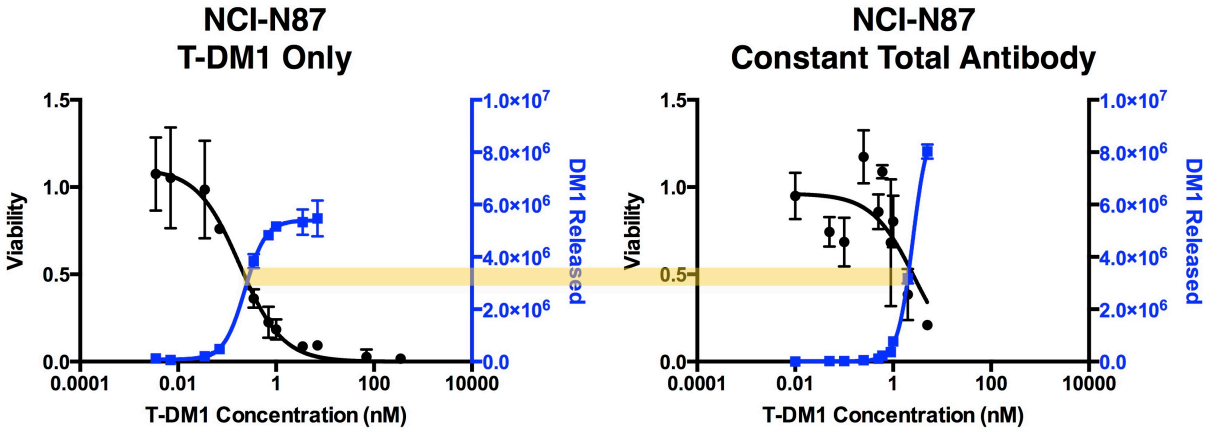

Figure S8 – NCI-N87 cell uptake and viability. Similar to other cytotoxicity assays, NCI-N87 cells were incubated with varying concentrations of T-DM1-680 for six days. Viability was measured using the PrestoBlue assay (Materials and Methods) and then cells were analyzed by flow cytometry to determine AF680 fluorescence signal. Quantitative beads were used to convert fluorescence signal to absolute number of molecules (and adjusting for the drug antibody ratio (DAR) and fluorophore degree of labeling (DoL). In both the T-DM1 alone and T-DM1 plus trastuzumab (constant 10 nM total antibody) cases, approximately 3.5 million molecules of DM1 are needed to achieve 50% cell killing. This agrees with Figure S17, where cell killing is determined by the amount of internalized T-DM1 and the amount of payload needed for cell death is not impacted by the presence or absence of trastuzumab.

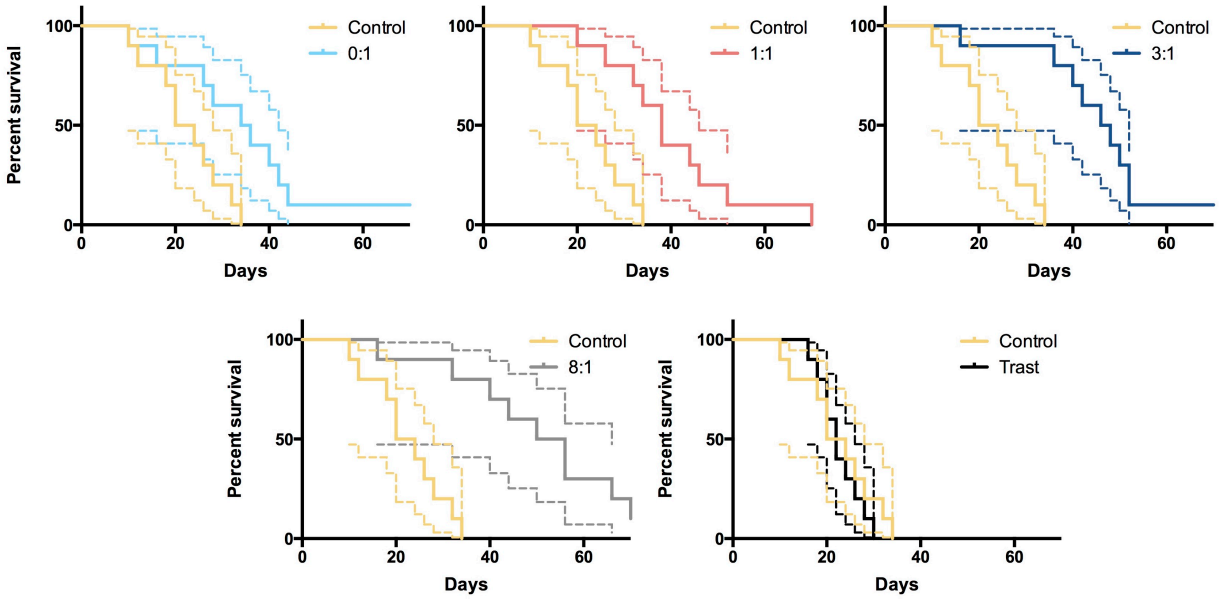

Figure S9 – Individual Kaplan-Meier curves with 95% confidence interval generated using PRISM software.

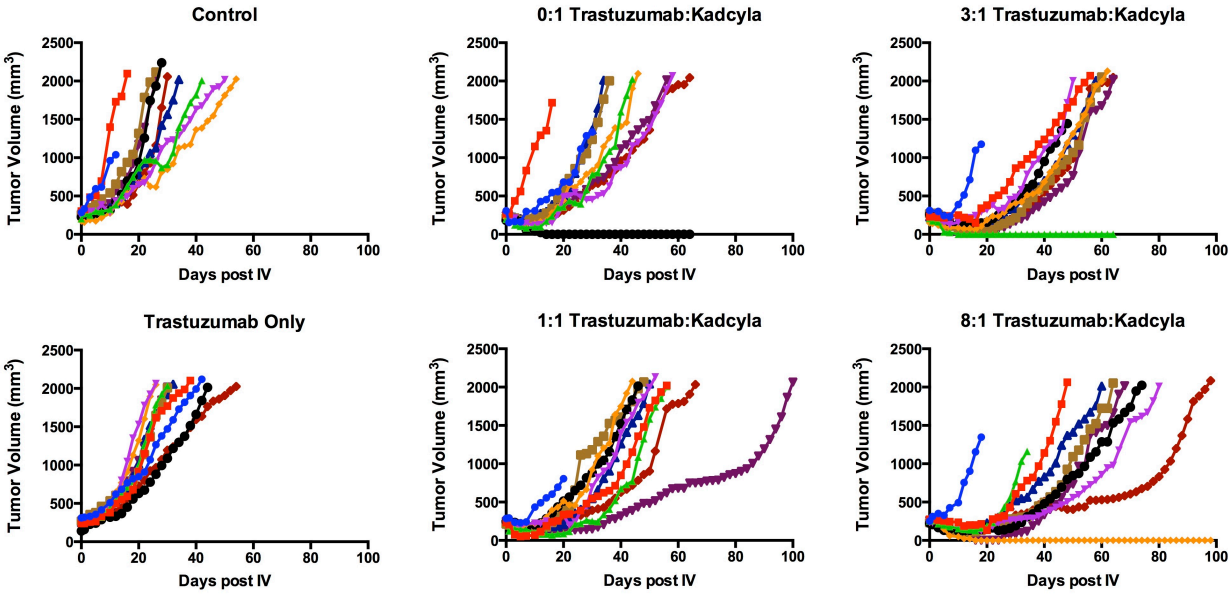

Figure S10 – Individual tumor growth curves for all animals.

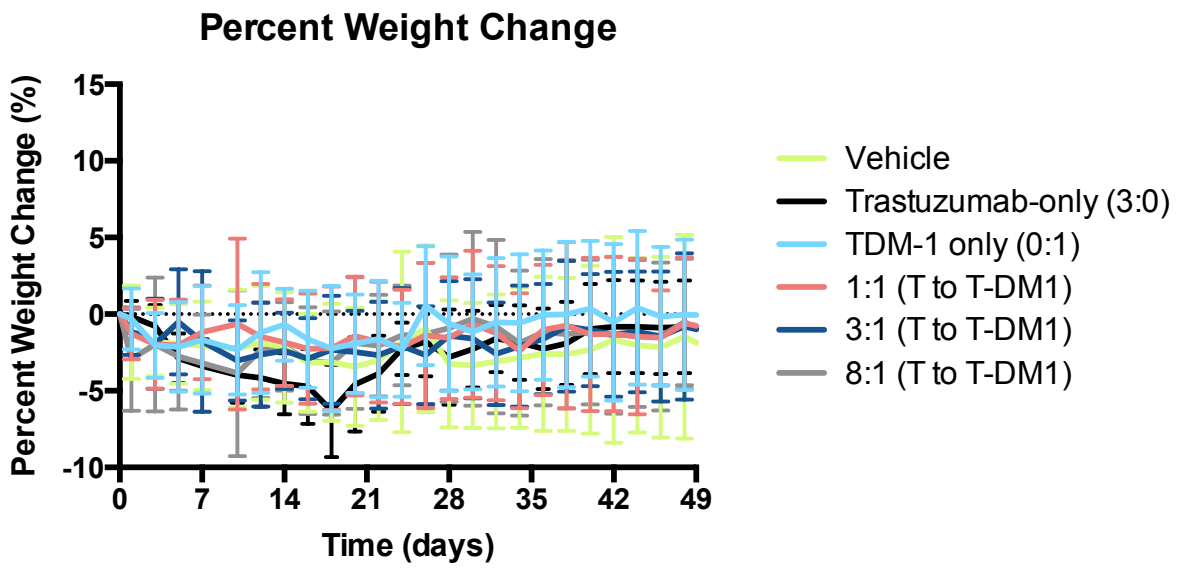

Figure S11 – Percent weight change during treatment. All treatments were well tolerated and no significant differences in mouse weight were encountered between treatments.

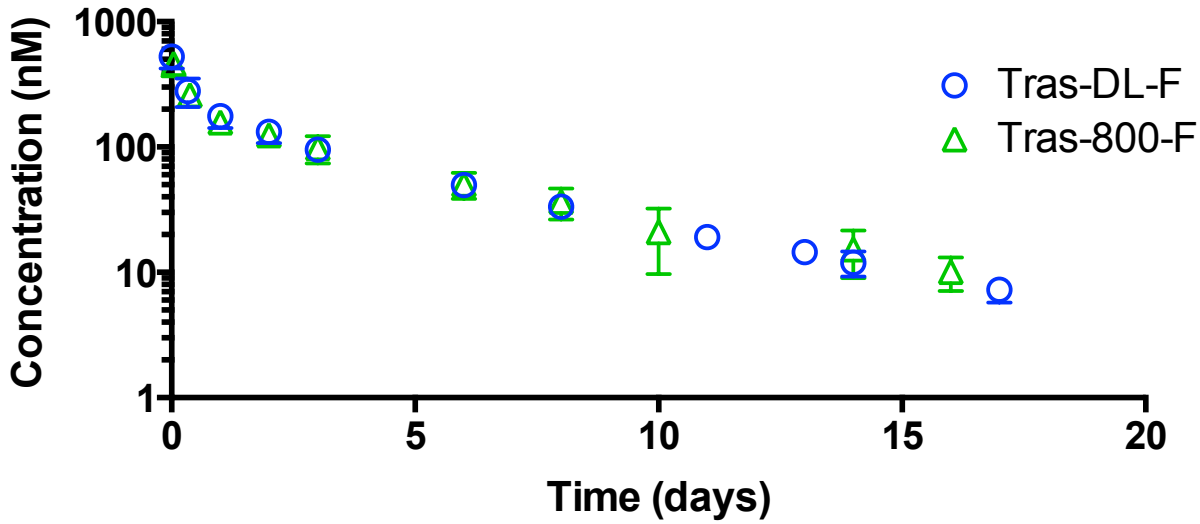

Figure S12 – Plasma clearance of dually labeled trastuzumab conjugate. In our previous work, we compared the clearance of trastuzumab-800 to unlabeled trastuzumab and found that trastuzumab-800 clearance was not significantly changed until 4 days post-injection(1). To ensure that conjugation of both DDAO and IRDye to the antibody does not alter clearance, we repeated this experiment and found that the clearance of dually labeled trastuzumab followed was identical to the clearance of trastuzumab-800 injected in a separate cohort of mice(1). This indicates that DDAO does not significantly impact clearance; dually labeled trastuzumab is cleared similarly to IRDye800CW labeled antibody and can be used for short-term (<4 days) pharmacokinetic studies. DL, dual-label (both IRDye and DDAO); 800, IRDye; F, fluorescence.

Supplementary Tables

A subtle but important point on matching efficacy to delivery is the role of cellular trafficking. The relationship between affinity, receptor saturation, and payload delivery is complicated by competition between trastuzumab and T-DM1 and the interdependence of trafficking and cell killing. For example, the uptake of DM1 (molecules per cell in Fig. 2A, B) plateaus at a lower concentration than the K_d,(17), indicating that cellular uptake is inhibited at higher concentrations of T-DM1, likely due to cell death. Importantly, when cells are saturated with antibody, which typically occurs around vessels *in vivo*, only a fraction of the receptors need to be occupied by T-DM1 (versus trastuzumab) for cell death (Fig. 2C, D). It appears that 50% cell death occurs with only 5% of the receptors occupied with T-DM1. Because of the potential differences *in vitro* versus *in vivo*, we used a NIR fluorescence ratio approach to quantify the cellular-level targeting and ADC payload delivery *in vivo* (Fig. 4, 5) in addition to *in vitro* (below).

HCC-1954 Cells

Time (hr)	Antibodies Uptake (antibody per cell)	Percent Intact Antibody (%)	DM1 Payload Released (molecules / cell)
0	$9.90 \times 10^5 \pm 1.2 \times 10^4$	100	0
3	$7.33 \times 10^5 \pm 3.6 \times 10^4$	92	$2.0 \times 10^5 \pm 3 \times 10^3$
6	$6.05 \times 10^5 \pm 7.0 \times 10^3$	86	$3.0 \times 10^5 \pm 4 \times 10^3$
12	$3.90 \times 10^5 \pm 1.4 \times 10^4$	69	$4.3 \times 10^5 \pm 2 \times 10^4$
18	$3.31 \times 10^5 \pm 1.1 \times 10^4$	41	$6.8 \times 10^5 \pm 2 \times 10^4$
24	$2.55 \times 10^5 \pm 2.6 \times 10^3$	29	$6.3 \times 10^5 \pm 7 \times 10^3$
36	$1.83 \times 10^5 \pm 7.0 \times 10^3$	23	$4.9 \times 10^5 \pm 2 \times 10^4$
48	$1.21 \times 10^5 \pm 3.6 \times 10^3$	11	$3.7 \times 10^5 \pm 1 \times 10^4$

Table S1 – Quantitative uptake, percent intact, and DM1 molecules released *in vitro* from dual label assay for HCC1954 cells.

NCI-N87 Cells

Time (hr)	Antibodies Uptake (antibody per cell)	Percent Intact Antibody (%)	DM1 Payload Released (molecules / cell)
0	$6.32 \times 10^5 \pm 1.3 \times 10^4$	100	0
3	$5.67 \times 10^5 \pm 1.4 \times 10^4$	91	$1.7 \times 10^5 \pm 4 \times 10^3$
6	$5.89 \times 10^5 \pm 1.6 \times 10^4$	88	$2.4 \times 10^5 \pm 7 \times 10^3$
12	$4.18 \times 10^5 \pm 3.4 \times 10^4$	80	$2.9 \times 10^5 \pm 2 \times 10^4$
18	$4.07 \times 10^5 \pm 8.0 \times 10^3$	61	$5.5 \times 10^5 \pm 1 \times 10^4$
24	$2.67 \times 10^5 \pm 2.0 \times 10^4$	47	$5.0 \times 10^5 \pm 4 \times 10^4$
36	$2.23 \times 10^5 \pm 1.2 \times 10^4$	39	$4.9 \times 10^5 \pm 2 \times 10^4$
48	$2.11 \times 10^5 \pm 2.9 \times 10^3$	33	$5.0 \times 10^5 \pm 1 \times 10^3$

Table S2 – Quantitative uptake, percent intact, and DM1 molecules released *in vitro* from dual label assay for NCI-N87 cells.

Supplementary Methods

Immunofluorescence Histology

Trastuzumab and Alexa Fluor 680 labeled T-DM1 (T-DM1-680) were administered via tail-vein at 0:1, 3:1, and 8:1 ratios (0, 10.8, and 28.8 mg/kg unlabeled trastuzumab with a constant 3.6 mg/kg T-DM1-680). Additionally, 15 minutes prior to sacrifice Hoechst 33342 (ThermoFisher Scientific, H3570) was injected via tail-vein at 15 mg/kg to labeled functional vasculature(3). 24 hours post-injection animals were euthanized, tumors were resected, flash frozen in OCT, and cut into 16 μm slices for histology. Before imaging, slides were stained for 25 minutes with antimouse CD31-AF555 and antihuman IgG Fc-AF488, or trastuzumab-AF750. The CD31 stain was used to calculate the total vessel surface area, and an automated image analysis program identified which CD31 stained vessels were adjacent to Hoechst stained cells (functional vessels), ADC-stained cells, or both to calculate the fraction of functional vessels that delivered ADC.

Image Analysis

Imaging tumors following treatment can provide insight into tumor relapse and regrowth between therapies (once every 3 weeks for T-DM1). The residualizing nature of the IRDye 800CW and AF680 labels on T-DM1 provide a history of which cells received the payload. Co-injection of Hoechst 33342 labels the functional vessels at the time of tumor resection. To determine impacts of the tumor vasculature (which both supplies oxygen and nutrients for tumor growth but also drugs for cell killing), we imaged tumors 1 and 5 days after treatment with 3.6 mg/kg of T-DM1. Significant mismatch between the functional vessels (Hoechst labeled) and treated regions (perivascular T-DM1) appeared at 5 days. To quantify these results, we used an automated image analysis algorithm to calculate the absolute vessel surface area to tumor volume ratio (S/V) along with the fraction of these vessels that had Hoechst and/or T-DM1 signal around them.

In order to find the surface-volume ratio, standard stereology methods were used on tumor xenograft images(4). Briefly, random 'lines' were placed on histological images (5 images per tumor and 4 (day 5) or 5 (day 1) tumors per condition) and the number of 'cuts' of the vessels was counted to yield the surface of the blood vessels- tumor volume ratio (S/V) as determined from Equation 1(5,6).

$$\frac{S}{V} = \frac{2c}{Ln} \qquad (1)$$

Where: c: cuts, L: length of lines (μm), n: number of lines.

A MATLAB code to automate this counting was created. Briefly, the three image channels representing the vessels, the intravenously delivered Hoechst signal (for functional vessels), and the antibodies were uploaded to the MATLAB script. A binary mask was generated to identify signal from background, and noise was removed. 10,000 lines were randomly placed on the image (to increase accuracy(5)), and the

function checks for the number of 'cuts' from these lines across a vessel. The length of the line was also chosen to be small (71μm, equivalent to 50 pixels). The S/V for select images was calculated manually using 300 lines to ensure the code was accurate. Each cut is categorized as either cut from a vessel (total vascular density), a cut from a functional vessel (proximity to intravenously delivered Hoechst), a cut from a vessel that delivered ADC (proximity to intravenously delivered ADC), or cut from a functional vessel that delivered ADC (proximity to both intravenously delivered Hoechst and ADC). With all the cuts estimated, the respective S/V is calculated.

Supplementary Discussion – Bystander Effects

Despite distribution limitations, ADCs and antibodies have had great success in the clinic and further insight into mechanisms of how a heterogeneous tissue distribution is able to result in complete tumor eradication is needed. The NIR fluorescence ratio technique provides a convenient way to monitor the multiple stages of ADC delivery with single-cell resolution and absolute quantification of delivery (molecules/cell). The heterogeneous tissue delivery can be imaged through microscopy, the fraction of targeted cells can be quantified through flow cytometry (Fig. 1, 5, 6), and the kinetics of ADC degradation measured by ratio measurement on flow cytometry (Fig. 5). Differences in target expression, antigen processing, possible target shedding, competition with endogenous ligands, accessibility (such as mucin blocking binding), and other mechanisms make the tumor distribution and development of each ADC uniquely challenging. Understanding these kinetics is crucial for developing ADCs since the majority release their toxic payload after degradation, and cell trafficking is a potential mechanism of resistance(7).

Similarly, the impact of payloads with bystander effects, which are not present in the T-DM1/trastuzumab model, is not completely defined. Intuitively, bystander effects would improve efficacy because therapeutic payload would reach cells beyond the penetration distance of the ADC (in addition to the benefit of targeting antigen negative cells). For example, tumor penetration issues may explain why similar antibody doses but higher DAR (and therefore a higher toxic payload dose) did not improve efficacy in several animal models(8-10) using agents without bystander effects. The higher DAR delivers more payload to cells that are already receiving a toxic dose, resulting in "overkill" of these cells. However, this same scenario with a payload that exhibits bystander effects shows improved efficacy(11-13). Although the payload is delivered to the same cells, it has the ability to diffuse into adjacent cells to improve overall cell killing. Consistent with our results, several groups(11,12,14) have shown greater efficacy with increased antibody-driven penetration (greater total antibody dose but same payload dose) even with payloads that exhibit bystander effects. For these payloads, it appears that the dilution and washout of the free payload may prevent the same efficacy as antibody-driven penetration to reach cells far from vessels.

References

1. Cilliers C, Nessler I, Christodolu N, Thurber GM. Tracking Antibody Distribution with Near-Infrared Fluorescent Dyes: Impact of Dye Structure and Degree of Labeling on Plasma Clearance. Mol Pharm **2017**;14:1623-33
2. Zhang L, Navaratna T, Thurber GM. A Helix-Stabilizing Linker Improves Subcutaneous Bioavailability of a Helical Peptide Independent of Linker Lipophilicity. Bioconjug Chem **2016**;27:1663-72
3. Trotter MJ, Chaplin DJ, Olive PL. Use of a Carbocyanine Dye as a Marker of Functional Vasculature in Murine Tumors. Br J Cancer **1989**;59:706-9
4. West MJ. Introduction to stereology. Cold Spring Harbor protocols **2012**;2012
5. Chalkley H, Cornfield J, Park H. A Method for Estimating Volume-Surface Ratios. Science **1949**;110:295-7
6. Hilmas D, Gillette E. Morphometric Analyses of the Microvasculature of Tumors During Growth and After X-Irradiation. Cancer **1974**;33:103-10
7. Loganzo F, Sung M, Gerber H-P. Mechanisms of Resistance to Antibody–Drug Conjugates. Mol Cancer Ther **2016**;15:2825-34
8. Sun X, Ponte JF, Yoder NC, Laleau R, Coccia J, Lanieri L*, et al.* Effects of Drug–Antibody Ratio on Pharmacokinetics, Biodistribution, Efficacy, and Tolerability of Antibody–Maytansinoid Conjugates. Bioconjug Chem **2017**;28:1371-81
9. Junutula JR, Flagella KM, Graham RA, Parsons KL, Ha E, Raab H*, et al.* Engineered thio-trastuzumab-DM1 conjugate with an improved therapeutic index to target human epidermal growth factor receptor 2-positive breast cancer. Clin Cancer Res **2010**;16:4769-78
10. Jackson D, Atkinson J, Guevara CI, Zhang C, Kery V, Moon SJ*, et al.* In vitro and in vivo evaluation of cysteine and site specific conjugated herceptin antibody-drug conjugates. PLoS One **2014**;9:e83865
11. Hamblett KJ, Senter PD, Chace DF, Sun MMC, Lenox J, Cerveny CG*, et al.* Effects of Drug Loading on the Antitumor Activity of a Monoclonal Antibody Drug Conjugate. Clin Cancer Res **2004**;10:7063-70
12. Pabst M, McDowell W, Manin A, Kyle A, Camper N, De Juan E*, et al.* Modulation of drug-linker design to enhance in vivo potency of homogeneous antibody-drug conjugates. J Control Release **2017**;253:160-4
13. Li F, Emmerton KK, Jonas M, Zhang X, Miyamoto JB, Setter JR*, et al.* Intracellular Released Payload Influences Potency and Bystander-Killing Effects of Antibody-Drug Conjugates in Preclinical Models. Cancer Res **2016**;76:2710-9
14. Junutula JR, Raab H, Clark S, Bhakta S, Leipold DD, Weir S*, et al.* Site-specific conjugation of a cytotoxic drug to an antibody improves the therapeutic index. Nat Biotechnol **2008**;26:925-32